Discreteness effects on a sine-Gordon breather

R. Boesch and M. Peyrard
Laboratoire Ondes et Structures Cohérentes, Faculté des Sciences, Université de Bourgogne
6 boulevard Gabriel, 21000 Dijon, France
(Received 18 October 1990)

We employ collective-variable theory to describe the dynamics of a breather excitation in its center-of-mass frame in continuous and discrete systems of one spatial dimension. The exact equations of motion for the collective variable and coupled phonon field are derived for any system which supports breatherlike excitations that have even spatial parity where the collective variable represents half the distance between the breather subkinks. We then specialize the theory to the sine-Gordon (SG) case. For the continuum SG system we derive the exact effective potential in terms of the collective variable and discuss the relativistic effects on the breather subkinks which are quite different than the relativistic effects on isolated boosted SG solitons. The effect of the subkink interaction is such that the subkinks do *not* Lorentz contract as they speed up when approaching the collision region (breather center). For the discrete SG breather system we derive expressions for the total energy, the effective potential which governs the motion of the breather subkinks, and a stability criterion for the breather's position relative to the lattice sites. We compare with simulation and find good agreement in most cases. Using molecular-dynamics and Fourier-transform techniques, we show that discrete SG breathers spontaneously make remarkably sharp transitions from a short lifetime to a long lifetime. The breather lifetimes on each side of the transition differ by more than four orders of magnitude. We relate the existence of the transition to the structure of the system's frequency spectrum. We also study the frequency spectrum of a "static" breather whose subkinks are trapped by the Peierls potential, yet are close enough to interact. For the latter case we illustrate the connection between collective-variable theory and standard perturbation analysis.

I. INTRODUCTION

There exist many one-dimensional nonlinear systems which support stable kink structures such as the sine-Gordon (SG),[1–10] double sine-Gordon,[11,12] modified sine-Gordon,[13,14] ϕ^4,[4,15] double-quadratic,[16,17] and multi-quadratic[18] systems, to name a few. It is well known that the high stability of the single-kink structures in these systems arises because of topological reasons. For example, if the field in any of the above systems approaches appropriate different asymptotic values as $x \rightarrow \pm\infty$, then the nonlinearity focuses the variation in the field until it is balanced by the dispersive effects giving rise to a kink structure. However, in order to create additional kink structures in these types of systems while at the same time leaving the boundary conditions unchanged, it is necessary to create kink-antikink pairs.

The energy required to create a kink-antikink pair such that the kink and antikink separate to infinity is at least twice the rest mass of a single kink. If an energy less than twice the rest mass is injected into the system by some means, then the kink-antikink pair may still be created but in this case the pair remains bound, i.e., a breather or breatherlike state is formed. It is apparent that, at low temperatures, the breathers will play a dominant role in the thermodynamics of kink-bearing systems since breather modes are easier to excite than kink modes. In fact, it has been shown[19,20] that breather dynamics make the dominant contributions at low temperatures to appropriate static and dynamic correlation functions. Therefore, considerable attention has been given to the role of continuum breathers in classical[21–24] and statistical[25] dynamics of nonlinear systems in the past decade. There has been some work carried out on the statistical dynamics of discrete systems but they treat gases of kinks.[26,27] The thermodynamics of discrete systems in which breathers are explicitly taken into account has not been treated. However, recent molecular-dynamics simulations which use a discrete SG system as a simple model for DNA suggest that the nucleation of kink-antikink pairs is a necessary precursor to localized denaturation of the DNA strand.[28]

On a completely different tack, the route to chaos of driven sine-Gordon continuum breathers has recently been treated in a collective-variable setting (neglecting phonons) by Taki *et al.*[23] Driven discrete breathers have not yet been treated.

There are, therefore, at least two lines of current research for which the generalization of the current theories to discrete-breather-bearing systems is natural. Indeed, it has already been shown[29] that the low-amplitude modes trapped by impurities in a discrete SG lattice are, in fact, low-amplitude breather modes. In addition, when such modes are unstable, the impurity "emits" two counterpropagating SG breathers. In Ref. 24 the asymptotic solution for a small-amplitude breather envelope whose frequency lies *above* but near the upper phonon band edge in a discrete system was obtained, although its stability was not analyzed.

It is for these reasons that we report our results on the

dynamics of discrete breathers where our explicit calculations are carried out for the SG system. In the present paper, we do not consider the thermodynamics of the system, nor do we consider a driven, damped discrete breather. We ask a more basic question: how are the dynamics of a free breather modified by discreteness? We only consider a breather whose frequency lies in the gap below the phonon band.

There are two major effects present which cause the discrete-breather system to exhibit fundamentally new dynamics. As is well known, the lifting of the spatial degeneracy in a discrete chain gives rise to the Peierls potential whose effects on the dynamics of single kinks have been studied extensively.[1,5–7,9,10,30] What is added in the breather system we consider is the competition between the Peierls energy and the subkink interaction energy. In addition, there exist harmonics of the breather motion which couple to the phonon modes and produce phonon radiation causing the breather motion to be damped thereby requiring the determination of the breather lifetime.

In general, we consider the discrete breather system such that the center of mass of the breather is at rest in the laboratory frame. We therefore focus primarily on the internal breathing motion and not the center-of-mass motion. In order to analytically calculate the effects due to discreteness, we employ collective-variable theory where the collective variable describes half the separation between the subkinks of the breather. Using a recently developed projection technique,[31–33] in Sec. II A we derive the exact coupled equations of motion for the collective variable and phonon field for a continuum breather system. In Sec. II B we then specialize the continuum theory to the SG case. We present the exact expression for the effective potential as a function of subkink separation for subkinks of the continuum breather and discuss the role played by this effective potential on the relativistic properties of the subkinks. Its effect is to exactly cancel the Lorentz contraction of the subkinks as they speed up when approaching the collision region.

In Sec. III A we derive the general collective-variable theory for a discrete-breather system and in Sec. III B apply it to the discrete SG case. We derive expressions for the total energy of the system and the effective potential for the collective variable, both of which explicitly describe the competition between the Peierls' wells and the subkink interaction energy. The theory indicates at which separations it is possible for the breather subkinks to become trapped. We call a discrete breather whose subkinks are trapped a "static breather" and in Sec. III C we determine the eigenfrequency spectrum of small oscillations about the static-breather profile by relating collective variable theory to standard perturbation analysis and then comparing with simulation.

We devote Sec. IV entirely to cases where the breather is not static but instead oscillates in the conventional breather fashion (modulo discreteness effects) for a wide range of breather frequencies. We present a numerical analysis of the frequency spectrum and show that discrete breathers spontaneously make remarkably sharp transitions from short lifetime to long lifetime where the increase in lifetime is more than four orders of magnitude. We relate the existence of this transition to the symmetry of the system and the structure of the frequency spectrum. We discuss the implications of our analysis on the stability of the discrete SG breather and compare with the stability predictions from collective-variable theory. In Sec. V we present our concluding remarks.

II. GENERAL CONTINUUM THEORY

A. Collective-variable theory for a continuum breather mode

We consider a field $\phi(x,t)$ in $1+1$ dimensions subjected to a substrate potential having the general form $V_{\rm sub}[\phi(x,t),x]$. The potential $V_{\rm sub}$ represents any potential which supports stable topological kink solutions. For example, $V_{\rm sub}$ may represent the SG potential with an impurity or a perturbed ϕ^4 potential. We assume that a breatherlike mode exists in the system. We define the continuum Hamiltonian density in dimensionless units where the speed of sound is set equal to unity as

$$\mathcal{H}=\tfrac{1}{2}\Pi^2+\tfrac{1}{2}\phi_x^2+V_{\rm sub}[\phi(x,t),x]\ , \tag{2.1}$$

where the field-momentum conjugate to ϕ is $\Pi(x,t)\equiv\dot{\phi}(x,t)$. The dynamics of the system are then given by the equation of motion

$$\ddot{\phi}-\phi_{xx}=-\frac{\partial V_{\rm sub}}{\partial\phi}\ . \tag{2.2}$$

Since we assume that the system supports a breatherlike mode, we introduce another set of variables in an effort to simplify the description of the dynamics. We let the fixed parameter X denote the center of mass of the breather in the system. The two subkinks which comprise the breather are each located a distance $z(t)$ from X, one subkink on each side, i.e., the subkinks are separated by a distance $2z(t)$, see Fig. 1. Thus, for the majority of cases considered in the present paper, we assume fixed X, thereby concentrating on the dynamics of the breather's internal mode. The only time we consider X to be time dependent is in Sec. III C when we treat the small-oscillations problem of the discrete system about a breather profile whose subkinks are trapped. We therefore treat cases for which $V_{\rm sub}[\phi(x,t),x]$ is such that the breather field is symmetric with even parity about the

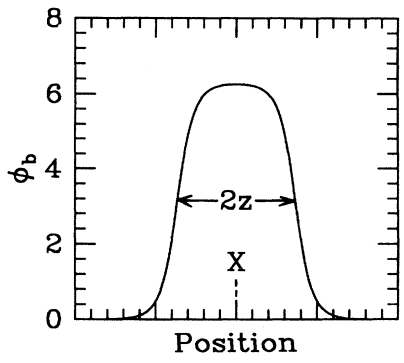

FIG. 1. Typical breather profile showing the meaning of the collective variable z and the parameter X.

breather center. In a full collective-variable treatment where X is assumed time dependent and not restricted to small displacements, then we must have that the collective variable z is a function of space as well as time, i.e., $z \equiv z(x,t)$, in order to account fully for relativistic effects associated with the center-of-mass motion. It is not necessary to include these effects for the purposes of the present paper.

We next decompose the field ϕ in the following way:[6,7,32,33]

$$\phi(x,t)=\sigma[x-X,z(t)]+\chi(x,t) , \tag{2.3a}$$

where σ is an ansatz function that reasonably approximates for a suitable choice of z for each t the profile of the actual system and χ, in general, accounts for the dressing of σ and any phonon radiation generated by the breather motion. By dressing we mean that part of $\chi(x,t)$ that is localized about the kinks in σ. One may choose σ to be the exact-breather profile of the system in the absence of perturbations if one exists. If an exact-breather solution in the absence of perturbations is not known, as in the ϕ^4 case, then it is reasonable to assume that an approximate-breather profile is given by a superposition of a kink and an antikink

$$\sigma_{K\bar{K}}[x-X,z(t)]=S(x-X+z)-S(x-X-z) , \tag{2.3b}$$

where $S(x)$ is an appropriate single-kink profile. The function χ though is extremely important in a case for which Eq. (2.3b) is the ansatz because $\sigma_{K\bar{K}}$ will need a large amount of dressing to correctly describe the profile when the subkinks are near each other.

Equation (2.3a) is the coordinate transformation from the field $\phi(x,t)$ to the collective-variable system consisting of the field $\chi(x,t)$ and the variable $z(t)$. We have therefore introduced into the Hamiltonian system two extra degrees of freedom in phase space [$z(t)$ and its conjugate momentum $P(t)$] and so we impose the two constraints

$$C_1=\langle\sigma'|\chi\rangle=0 , \tag{2.4a}$$

$$C_2=\langle\sigma'|\pi\rangle=0 , \tag{2.4b}$$

in order to conserve the number of degrees of freedom. The function $\pi(x,t)$ is the momentum conjugate to $\chi(x,t)$ and the prime denotes the derivative with respect to z. The bracket notation means integration over dx from $-\infty$ to ∞. The first constraint gives meaning to the variable $z(t)$ by determining z such that σ is the best fit to the shape of the actual breather system. The choice of the second constraint imposes a condition[33(b)] on the momentum transformation [cf. Eq. (2.5f)] from the momentum $\Pi(x,t)$ to the momenta $\pi(x,t)$ and P such that the collective-variable Hamiltonian H takes the following form:

$$H=\frac{P^2}{2\bar{M}_z}+\tfrac{1}{2}\langle\pi|\pi\rangle+\tfrac{1}{2}\bar{M}_X+\tfrac{1}{2}\langle\chi_x|\chi_x\rangle-\frac{M_X}{2}b_X^2 + \int_{-\infty}^{\infty} dx\, V_{\rm sub}(\sigma+\chi) , \tag{2.5a}$$

where

$$M_z\equiv\langle\sigma'|\sigma'\rangle, \quad M_X\equiv\langle\sigma_x|\sigma_x\rangle=\left\langle\frac{\partial\sigma}{\partial X}\middle|\frac{\partial\sigma}{\partial X}\right\rangle \tag{2.5b}$$

are the masses associated with the z mode and the center-of-mass mode, respectively, and

$$\bar{M}_z\equiv M_z(1-b_z)^2, \quad b_z\equiv\frac{1}{M_z}\langle\sigma''|\chi\rangle , \tag{2.5c}$$

$$\bar{M}_X\equiv M_X(1-b_X)^2, \quad b_X\equiv\frac{1}{M_X}\left\langle\frac{\partial^2\sigma}{\partial X^2}\middle|\chi\right\rangle , \tag{2.5d}$$

$$\pi(x,t)=\dot{\chi}(x,t)+b_z\dot{z}\sigma', \quad P=\bar{M}_z\dot{z} , \tag{2.5e}$$

$$\Pi(x,t)=\frac{P\sigma'}{M_z(1-b_z)}+\pi(x,t) . \tag{2.5f}$$

Note that only the subscripts on σ and χ denote partial derivatives. The subscripts on the other quantities, such as M_X and b_z, are only labels for these functions defined in Eq. (2.5).

We see that the kinetic energy of the collective mode appears explicitly as the first term in Eq. (2.5a). If the constraint C_2 is chosen differently, the kinetic energy of the collective mode does not separate conveniently from the rest of the Hamiltonian but is inconveniently accounted for in more than one term. The second term in H is, in general, the kinetic energy of the phonon and dressing field. The next three terms arise from the elastic coupling energy. Even though we are considering the system such that its center of mass is at rest, the mass $M_X(z)$ associated with the center-of-mass motion appears in H because $\partial\sigma/\partial x=-\partial\sigma/\partial X$.

It is possible to derive the coupled equations of motion for $\ddot{\chi}$ and $\ddot{z}$ in two ways. One way requires much calculation and consists of using the Dirac bracket—Dirac's generalization of the Poisson bracket in the presence of constraints—to calculate from H in Eq. (2.5a) the first-order equations of motion for the system of coordinates z and χ, and momenta P and π, after which the momenta must be eliminated. One ultimately obtains two coupled equations of motion for the collective variable $z(t)$ and the phonon-dressing field $\chi(x,t)$ which are exact relative to the constraints and second order in time. From this coupled pair of equations, one calculates the effective potential for z. However, one of the most useful results of collective-variable theory is that the above procedure for the derivation of the collective-variable equations of motion is equivalent to a simple projection-operator technique. The derivation of the equations of motion using the projection algorithm is then carried out very quickly and requires that we first substitute the ansatz Eq. (2.3a) into Eq. (2.2) to obtain one equation of motion of the pair. Second, we project this equation of motion in the direction σ' to obtain the other equation of motion of the pair. See Ref. 33(a) for the proof of the equivalence of the two methods.

Substituting Eq. (2.3a) into Eq. (2.2) we obtain

$$\ddot{\chi}-\chi_{xx}+\sigma'\ddot{z}+\sigma''\dot{z}^2-\sigma_{xx}=-\frac{\partial V_{\rm sub}(\sigma+\chi)}{\partial\sigma} . \tag{2.6a}$$

Next, projecting Eq. (2.6a) in the direction σ' (integrating over x) we obtain, after dividing through by $M_z(z)$,

$$\ddot{z}+\frac{1}{2}\frac{\partial \ln M_z}{\partial z}\dot{z}^2-\frac{1}{M_z}\langle\sigma'|\sigma_{xx}\rangle=-\frac{1}{M_z}\langle\sigma'|\ddot{\chi}\rangle+\frac{1}{M_z}\langle\sigma'|\chi_{xx}\rangle-\frac{1}{M_z}\left\langle\sigma'\left|\frac{\partial V_{\rm sub}(\sigma+\chi)}{\partial\sigma}\right\rangle\right. . \tag{2.6b}$$

The coupled equations of motion (2.6a) and (2.6b) are exact and completely determine the evolution of the symmetric breather system in terms of the variable $z(t)$ and the field $\chi(x,t)$. The constraints $C_1=0$ and $C_2=0$ must be satisfied initially; the theory then guarantees they are satisfied for all time as long as the dynamics evolve according to Eqs. (2.6a) and (2.6b).

At this stage of the theory an expansion in χ can be made in order to calculate, say, the linear dressing of the function σ where the corrected σ may, for example, be used to calculate corrected (renormalized) frequencies of characteristic oscillations of the system and their corresponding radiation linewidths such as in the case of the quasimode for a SG soliton.[9] In addition, the Hamiltonian Eq. (2.5a) can be expanded in χ in order to investigate the role of phonon interactions in the statistical mechanics of the system.[34] Note that if χ is set to zero, then the "bare" theory results. The bare theory may or may not agree well with simulation depending on the choice of σ; that is, depending on how much dressing χ has been thrown away. In the next subsection we apply the above theory to the continuum SG case so that we can compare with the discrete generalization of the theory derived in Sec. III.

B. Continuum sine-Gordon breather system

We consider the continuum SG system where

$$V_{\rm sub}[\phi(x,t),x]=V_{\rm SG}[\phi(x,t)]\equiv\Gamma_0^2(1-\cos\phi) . \tag{2.7}$$

Equation (2.2) thus becomes

$$\ddot{\phi}-\phi_{xx}+\Gamma_0^2\sin\phi=0 . \tag{2.8}$$

The meaning of the parameter Γ_0 is made clear by expanding ϕ about the vacuum solution as

$$\phi_\epsilon=\epsilon\exp i(kx-\omega t) ,$$

where ϵ is a small parameter, substituting ϕ_ϵ into Eq. (2.8) and linearizing in ϵ in order to obtain the phonon dispersion law

$$\omega^2=k^2+\Gamma_0^2 . \tag{2.9}$$

Therefore, the parameter Γ_0 is the frequency of the $k=0$ phonon, or equivalently, the frequency of the phonon band edge.

The single-soliton solution of Eq. (2.8) in its center-of-mass frame is

$$\phi_s=4\tan^{-1}\exp[\Gamma_0(x-X_s)] , \tag{2.10}$$

where X_s locates the center of mass of the soliton. The breather solution in its center-of-mass frame is

$$\phi_b=4\tan^{-1}\left[\frac{k_b\cos(\omega_b t-\theta)}{\omega_b\cosh[k_b(x-X)]}\right] , \tag{2.11}$$

where X locates the center of mass of the breather, the parameter θ determines the initial phase, ω_b is the breather frequency, and ω_b and k_b satisfy

$$\omega_b^2+k_b^2=\Gamma_0^2 . \tag{2.12}$$

From Eq. (2.12) we see that Γ_0 also represents the maximum allowed breather frequency.

We next express the breather solution Eq. (2.11) as the sum of a kink and an antikink—which is *not* an approximation but a rigorous result for the continuum SG breather system. Defining $z(t)$ as

$$\sinh[k_b z(t)]\equiv\frac{k_b}{\omega_b}\cos(\omega_b t-\theta) \tag{2.13}$$

and substituting Eq. (2.13) into Eq. (2.11), we obtain

$$\begin{aligned}\phi_b&=4\tan^{-1}\left[\frac{\sinh(k_b z)}{\cosh[k_b(x-X)]}\right]\\&=4\tan^{-1}\exp[k_b(x+z-X)]\\&\quad-4\tan^{-1}\exp[k_b(x-z-X)] .\end{aligned} \tag{2.14}$$

Equation (2.14) implies that the exact SG breather consists of a linear superposition of a kink and an antikink which are separated by a distance $2z(t)$ which is centered on X. (See Refs. 11, 12, 23, 34, and 35 for similar collective-coordinate descriptions.) Equations (2.13) and (2.14) imply that the breather motion corresponds to the subkinks oscillating about the center of mass of the system where oscillations of larger amplitude in $z(t)$ correspond to lower frequencies. Note that the subkinks of the breather given by the right-hand side of Eq. (2.14) are *not* the same as the single-soliton solutions of Eq. (2.8) since the spatial extent of each subkink in Eq. (2.14) is given approximately by $2/k_b$ and not by $2/\Gamma_0$ as in Eq. (2.10). However, the subkinks asymptotically approach the soliton solution of Eq. (2.10) in the limit $z\to\infty$, assuming they have enough energy to do so, because this limit corresponds by Eq. (2.13) to very low-frequency breathers which, in turn, implies by Eq. (2.12) that $k_b\to\Gamma_0$.

Next, we substitute $\sigma=\phi_b$ into the Hamiltonian Eq. (2.5a) (which implies $\chi=\pi=0$ because ϕ_b is the exact SG breather solution) and the Hamiltonian becomes

$$H_{\rm SG}(z,P)=\frac{P^2}{2M_z(z)}+V(z) , \tag{2.15a}$$

$$V(z)=\tfrac{1}{2}M_z(z)\left[\frac{\Gamma_0}{k_b}\tanh(k_b z)\right]^2+\tfrac{1}{2}M_\chi(z) , \tag{2.15b}$$

where

$$M_z(z)=16k_b\left[1+\frac{2k_bz}{\sinh(2k_bz)}\right],$$
$$M_X(z)=16k_b\left[1-\frac{2k_bz}{\sinh(2k_bz)}\right], \tag{2.15c}$$

and

$$P=M_z\dot{z}\ . \tag{2.15d}$$

In deriving Eqs. (2.15a) and (2.15b) we used

$$\int_{-\infty}^{\infty}dx\ V_{\rm SG}(\phi_b)=\tfrac{1}{2}M_z(z)\left[\frac{\Gamma_0}{k_b}\tanh(k_bz)\right]^2. \tag{2.15e}$$

It must be borne in mind that the masses $M_z(z)$ and $M_X(z)$ do not reflect much information about the individual effective masses of the breather subkinks (except in the large-z limit) but rather they are the effective masses associated with the z and X *modes*. The reason is because M_z and M_X do not account for velocity effects which we will discuss in more detail when we calculate the effective potential seen by the subkinks. For now, however, we just note that the masses M_z and M_X both approach $16\Gamma_0$ in the limit $z\to\infty$, where $16\Gamma_0$ is the total energy of the infinitely separated solitons whose profiles are given by Eq. (2.10). As $z\to 0$, we have $M_z\to 32k_b$ and $M_X\to 0$. In general, we note that the mass of the z mode is larger than the mass of the X mode, the difference arising because the subkinks have opposite helicities, as we will discuss in more detail in Sec. III C.

We now calculate the total energy of the system from the collective-variable Hamiltonian in Eq. (2.15a) merely in order to make contact with the previously well-known result of the energy of a SG breather. If we define the amplitude of the subkink oscillations as $z_0\equiv z(t=0)$, then we obtain from Eq. (2.13) with $\theta=0$ the result

$$\frac{\Gamma_0}{k_b}\tanh(k_bz_0)=1\ . \tag{2.16a}$$

Equation (2.16a) corresponds to the initial condition where the breather is started from rest

$$P_0\equiv P(t=0)=0 \tag{2.16b}$$

with the subkinks at their maximum separation z_0. Throughout the present paper we *always* consider the $t=0$ initial condition to be started from rest. Substituting Eqs. (2.16a) and (2.16b) into the Hamiltonian Eq. (2.15a), we obtain the total energy $E^c_{\rm tot}$ of the continuum system:

$$E^c_{\rm tot}=H_{\rm SG}(z_0,P_0)=\tfrac{1}{2}[M_z(z_0)+M_X(z_0)]=16k_b\ , \tag{2.16c}$$

where $16k_b$ is the well-known expression for the total energy of the continuum SG breather system in the center-of-mass frame.

Since $\chi=\pi=0$, the constraints are identically satisfied and the equation of motion for $\ddot{z}$ is derived by using the unconstrained Hamilton equations

$$\dot{z}=\frac{\partial H_{\rm SG}}{\partial P},\quad \dot{P}=-\frac{\partial H_{\rm SG}}{\partial z}\ , \tag{2.17}$$

or simply by reducing Eq. (2.6b) for the present case:

$$\ddot{z}+\frac{1}{2}\frac{\partial \ln M_z}{\partial z}\dot{z}^2=-\frac{1}{M_z}\frac{\partial V(z)}{\partial z}\ , \tag{2.18}$$

where $V(z)$ is given by Eq. (2.15b). Equation (2.18) is the exact equation of motion for the collective variable z for the continuum SG breather system and indicates that the general potential given in terms of the variable z is velocity dependent, i.e., the $\dot{z}^2$ term. However, we can obtain an effective potential in terms of z which takes into account all velocity effects by considering the first integral of Eq. (2.18) which is just the Hamiltonian given by Eq. (2.15):

$$\tfrac{1}{2}M_z(z)\dot{z}^2+V(z)=E^c_{\rm tot}=16k_b\ . \tag{2.19a}$$

We rewrite Eq. (2.19a) as

$$\tfrac{1}{2}\dot{z}^2+V_{\rm eff}(z)=0\ , \tag{2.19b}$$

where

$$V_{\rm eff}\equiv\frac{1}{M_z(z)}[V(z)-E_{\rm tot}]$$
$$=\frac{1}{2}\left[\frac{\Gamma_0}{k_b}\tanh(k_bz)\right]^2-\frac{1}{2}\ . \tag{2.19c}$$

Equation (2.19b) is an effective Hamiltonian for a particle of unit mass moving in the potential $V_{\rm eff}$ where the total effective energy is zero. Taking the time derivative of Eq. (2.19b), we obtain

$$\ddot{z}=-\frac{\partial V_{\rm eff}(z)}{\partial z}\ , \tag{2.19d}$$

which is a simple equation of motion for z that is equivalent to Eq. (2.18) since it is expressed in terms of $V_{\rm eff}(z)$. Note that, because of the complete integrability of the SG system, Eq. (2.19c) is exact for the collective variable z.

We see that $V_{\rm eff}(z)$, which has a width $\sim 2/k_b$, is an attractive potential [dotted line in Figs. 3(a) and 3(b)] indicating that the subkinks increase their velocities from zero as they approach one another. In fact, at the center of the interaction region ($z=0$), the velocity reaches the value $|\dot{z}|=1$ by Eqs. (2.19b) and (2.19c) and therefore the collision is ultrarelativistic. However, the right-hand side of Eq. (2.14) which is exact indicates that there is no Lorentz contraction of the subkinks as they approach the collision region—their widths $\sim 2/k_b$ are constant for all time. This constancy of the subkink mass is in marked contrast to that of a single boosted, but *isolated*, SG kink whose rest length undergoes a Lorentz contraction $\gamma^{-1}=(1-v^2)^{1/2}$, where v is the soliton's constant velocity. In general, that is, Γ_0 in Eq. (2.10) is multiplied by γ.

The subkinks have constant mass because of two effects, one which tends to increase the mass and the other tends to decrease the mass, which balance exactly. The "standard" relativistic increase in mass comes from the increase in kinetic energy near the collision region. However, unlike special relativity where the dilated particle mass is determined only by the particle's instantane-

ous velocity, the value of the local potential relative to the vacuum acting on the subkinks *also* affects the mass. This is seen by noting that breathers for different subkink separations z_0 correspond, respectively, at $t=0$ to subkinks of different widths $2/k_b$ simply because the initial strength of the subkink interaction is different for each z_0 case. The decrease in the potential near the collision region therefore decreases the subkink mass. Since the system conserves energy, the two opposed mass dilations exactly balance since no phonons are generated due to integrability.

We point out that the same effect is true for collisions between soliton-soliton or unbound soliton-antisoliton pairs. To obtain the effective potential for a soliton-antisoliton collision, let $k_b \rightarrow \gamma \Gamma_0$ in Eq. (2.19c) where the relativistic parameter γ is a function of the asymptotic velocity of the colliding solitons (i.e., at infinite separation) in the center-of-mass frame. For a soliton-soliton collision, make the same replacement and, in addition, let tanh$\rightarrow$coth. For a soliton-soliton collision, the potential near the collision region increases (i.e., a repulsive potential) and so the mass increases but the solitons simultaneously reduce their velocity and the Lorentz contraction therefore decreases leaving no net mass change in the colliding solitons. This also explains why a constant mass solution exists (neglecting phonons) for a SG soliton whose center of mass is oscillating in a parabolic potential well.[3]

Therefore, although SG solitons have been described as "relativistic particles" in the literature, it is not, in general, true that a SG soliton propagating at a nonzero velocity is Lorentz contracted from its rest width. One must take into account the change in the local effective potential and its effect on the soliton's mass. Therefore, although the SG equation, as well as its solutions, are Lorentz invariant, standard special-relativity arguments do not apply, in general, to the description of the dynamics of *interacting* solitons which *make up* the solution.

These considerations on the constancy of the soliton width during interaction, together with the exact pairwise interaction potential between solitons [cf. Eq. (2.19c)], suggest that it may be possible to construct a simple statistical-mechanical theory of an interacting SG soliton gas at low densities. Furthermore, if similar results hold for the three-soliton solution, it suggests that soliton gases at higher densities may also be treated. Work along these lines is in progress.

In closing this section we note the following result. Expanding Eq. (2.13) for the case $k_b z_0 \ll 1$ yields

$$z_0 = \frac{1}{\omega_b} \ . \tag{2.20}$$

Since the only requirement on ω_b is $\omega_b \leq \Gamma_0$, we obtain the general result that

$$z_0 \geq \frac{1}{\Gamma_0} \ . \tag{2.21}$$

According to Eq. (2.21), $1/\Gamma_0$ is a lower bound on the amplitude z_0 of the breather oscillation and so arbitrarily small oscillations of $z(t)$ *do not exist* in the continuum SG breather system. Of course, the amplitude of the field ϕ_b may be arbitrarily small since, by Eq. (2.14), it depends on $\sinh(k_b z_0)$ and $k_b \rightarrow 0$ as $z_0 \rightarrow 1/\Gamma_0$. For example, we note that, if we choose $z_0 = 1/\Gamma_0$, then Eq. (2.16a) yields $k_b = 0$ as the only solution thus indicating that $\phi_b \rightarrow 0$ and the breather energy $E^c_{\rm tot} = 16 k_b \rightarrow 0$. The next section extends to discrete systems the results discussed above in the continuum limit.

III. GENERAL DISCRETE THEORY

A. Collective-variable theory for a discrete-breather mode

We consider a one-dimensional chain of harmonically coupled particles where the phase or position of the lth particle measured with respect to some reference is denoted by $Q_l(t)$. The system is subjected to a substrate potential of the general form $V_{\rm sub}[Q_l(t), l]$ such that the discrete breather maintains even parity in space.

The Hamiltonian for the system is

$$H = \tfrac{1}{2} \sum_l P_l^2 + \tfrac{1}{2} \sum_l (Q_{l+1} - Q_l)^2 + \sum_l V_{\rm sub}(Q_l) \ , \tag{3.1}$$

where the momentum P_l conjugate to Q_l is defined as $P_l \equiv \dot{Q}_l$. The corresponding equation of motion for $\ddot{Q}_l$ is

$$\ddot{Q}_l - \Delta_2 Q_l = -\frac{\partial V_{\rm sub}}{\partial Q_l} \ , \tag{3.2}$$

where $\Delta_2 Q_l \equiv Q_{l+1} + Q_{l-1} - 2Q_l$ denotes the second difference.

The incorporation of the collective variable $z(t)$ and the parameter X for the discrete case parallels the procedure in the previous section. We decompose the field Q_l as

$$Q_l = f[l - X, z(t)] + q_l(t) \ , \tag{3.3}$$

where f_l is the breather ansatz function and the field q_l accounts for the dressing of f_l and phonon radiation. The parameter X is fixed and so our analysis is valid for the case where the discrete breather is centered on a particle or centered between particles—there is no X motion.

We impose the two constraints

$$C_1 = \langle f_l' | q_l \rangle = 0 \ , \tag{3.4a}$$

$$C_2 = \langle f_l' | p_l \rangle = 0 \ , \tag{3.4b}$$

where p_l is the momentum conjugate to q_l, the prime denotes the derivative with respect to z and from now on the bracket notation means *sum over* l rather than integration over dx. The constraints for the discrete theory define the collective variable in exactly the same sense as in the previous section. We have the following correspondence: ϕ, Π, σ, χ, and π in Sec. II are now replaced by Q_l, P_l, f_l, q_l, and p_l, respectively.

Using the results of Ref. 33(a), the collective variable

Hamiltonian for the discrete breather system is

$$H^d=\frac{P^2}{2\overline{M}^{\,d}_z}+\tfrac{1}{2}\langle p_l|p_l\rangle+\tfrac{1}{2}\sum_l (f_{l+1}-f_l+q_{l+1}-q_l)^2 + \sum_l V_{\rm sub}(f_l+q_l)\ , \tag{3.5a}$$

where

$$M_z^d(z,X)=\langle f_l'|f_l'\rangle \tag{3.5b}$$

is the discrete generalization of the mass $M_z(z)$ [cf. Eq. (2.5b)] associated with the z motion and

$$\overline{M}^{\,d}_z\equiv M_z^d(1-b_z^d)^2,\quad b_z^d\equiv\frac{1}{M_z^d}\langle f_l''|q_l\rangle\ , \tag{3.5c}$$

$$p_l=\dot q_l+b_z^d\dot z f_l',\quad P=\overline{M}^{\,d}_z\dot z\ , \tag{3.5d}$$

$$P_l=\frac{Pf_l'}{M_z^d(1-b_z^d)}+p_l\ . \tag{3.5e}$$

Note that $M_z^d(z,X)$ is a function of X. We also observe that the mass $M_X^d(z,X)$, which is the discrete generalization of the mass $M_X(z)$ in Eq. (2.5b), does not appear in Eq. (3.5) because there are no derivatives with respect to x in H^d but only finite differences with respect to l.

The exact equations of motion of $\ddot q_l$ and $\ddot z$ are obtained by substituting the ansatz Eq. (3.3) into Eq. (3.2) which yields

$$\ddot q_l-\Delta_2 q_l+f_l'\ddot z+f_l''\dot z^2-\Delta_2 f_l=-\frac{\partial V_{\rm sub}}{\partial f_l} \tag{3.6a}$$

and then projecting Eq. (3.6a) in the direction f_l to obtain

$$\ddot z+\frac{1}{2}\frac{\partial \ln M_z^d}{\partial z}\dot z^2-\frac{1}{M_z^d}\langle f_l'|\Delta_2 f_l\rangle=-\frac{1}{M_z^d}\langle f_l'|\ddot q_l\rangle+\frac{1}{M_z^d}\langle f_l'|\Delta_2 q_l\rangle-\frac{1}{M_z^d}\left\langle f_l'\left|\frac{\partial V_{\rm sub}(f_l+q_l)}{\partial f_l}\right.\right\rangle\ . \tag{3.6b}$$

The equations of motion (3.6a) and (3.6b) are the discrete generalization of the continuum equations (2.6a) and (2.6b).

In order to obtain from the discrete theory a simple expression for the total energy of the breather (as a function of the initial subkink separation z_0 and X) and an expression for the effective potential for $z(t)$, we continue the analysis for the simpler "bare" case corresponding to $q_l=0$. The bare case is valid in the limit of large kink width (high-frequency breathers) since that is the limit in which the dressing and radiation effects are least.

B. Discrete sine-Gordon breather system

Choosing the ansatz function

$$f_l=4\tan^{-1}\left[\frac{\sinh(k_b z)}{\cosh[k_b(l-X)]}\right] \tag{3.7a}$$

and

$$V_{\rm sub}(f_l)=V_{\rm SG}(f_l)=\Gamma_0^2(1-\cos f_l)\ , \tag{3.7b}$$

a natural definition according to Eq. (3.5a) for the bare ($q_l=0$) potential for the discrete SG breather is

$$\mathcal{V}^d_{\rm bare}(z,X)=\tfrac{1}{2}\langle f_{l+1}-f_l|f_{l+1}-f_l\rangle+\sum_l V_{\rm SG}(f_l)\ . \tag{3.8a}$$

Equation (3.8a), however, is not accurate because, if we expand the finite difference in Eq. (3.8a) in a Taylor series and keep all the terms, we are essentially keeping higher and higher corrections to discreteness due to the f_l but at the same time we are neglecting the corrections due to the q_l which we have set to zero. The Taylor series expansion is not valid unless we simultaneously include corrections due to q_l at each order which is a rather formidable task in light of the fact that the breatherlike state is inherently time dependent. We can, however, gain significant insight as to how discreteness changes the breather dynamics by retaining the first term in the Taylor series.

We expand the finite difference in Eq. (3.8a) and consider the potential

$$V^d_{\rm bare}(z,X)=\frac{1}{2}\left\langle\frac{\partial f_l}{\partial l}\left|\frac{\partial f_l}{\partial l}\right.\right\rangle+\sum_l V_{\rm SG}(f_l)\ , \tag{3.8b}$$

where we have replaced $f_{l+1}-f_l$ by $\partial f_l/\partial l$. (Recall the bracket notation means *sum* on l.) We define the discrete generalization of $M_X(z)$ as

$$M_X^d(z,X)\equiv\left\langle\frac{\partial f_l}{\partial l}\left|\frac{\partial f_l}{\partial l}\right.\right\rangle \tag{3.9}$$

and further note that f_l satisfies

$$\sum_l V_{\rm SG}(f_l)=\tfrac{1}{2}M_z^d(z,X)\left[\frac{\Gamma_0}{k_b}\tanh(k_b z)\right]^2\ . \tag{3.10}$$

Upon substituting Eqs. (3.9) and (3.10) into Eq. (3.8b), we obtain the discrete bare Hamiltonian for the SG breather system:

$$H^d_{\rm bare}(z,X,P)=\frac{P^2}{2M_z^d}+V^d_{\rm bare}(z,X)\ , \tag{3.11a}$$

$$V^d_{\rm bare}(z,X)=\tfrac{1}{2}M_z^d(z,X)\left[\frac{\Gamma_0}{k_b}\tanh(k_b z)\right]^2+\tfrac{1}{2}M_X^d(z,X)\ , \tag{3.11b}$$

$$P=M_z^d(z,X)\dot z\ . \tag{3.11c}$$

We see that the form of $H^d_{\rm bare}$ in Eq. (3.11) is identical to the form of the continuum Hamiltonian $H_{\rm SG}$ in Eqs. (2.15a) and (2.15b) but that discreteness in $H^d_{\rm bare}$ enters in

through the masses $M_z^d(z,X)$ and $M_X^d(z,X)$. We now derive expressions for these masses and, consequently, the total energy of the system.

We note that both masses are periodic in X with period unity and therefore we expand M_z^d and M_X^d in a Fourier series in X. It was shown in Ref. 6 that, for a function of the form $\sum_l g(l-X)$, the Fourier coefficients in the Fourier series

$$\sum_l g(l-X)=\frac{A_0}{2}+\sum_{n=1}^{\infty} A_n\cos(2\pi nX) + \sum_{m=0}^{\infty} B_m\sin(2\pi mX) \tag{3.12a}$$

are given by

$$A_n=2\int_{-\infty}^{\infty} g(u)\cos(2\pi nu)du, \quad n=0,1,\ldots, \tag{3.12b}$$

$$B_m=-2\int_{-\infty}^{\infty} g(u)\sin(2\pi mu)du, \quad m=1,2,\ldots. \tag{3.12c}$$

We therefore find

$$M_z^d(z,X)=M_z(z)+\sum_{n=1}^{\infty} A_n^z(z)\cos(2\pi nX)\ , \tag{3.13a}$$

$$M_X^d(z,X)=M_X(z)+\sum_{n=1}^{\infty} A_n^X(z)\cos(2\pi nX)\ , \tag{3.13b}$$

where the coefficients A_n^z and A_n^X are given by

$$\begin{bmatrix} A_n^z(z) \\ A_n^X(z) \end{bmatrix} = \frac{32\pi k_b}{\sinh(\pi^2 n/k_b)} \times \left[\frac{n\pi}{k_b}\cos(2\pi nz)\right] \begin{bmatrix} + \\ - \end{bmatrix} \frac{\sin(2\pi nz)}{\sinh(2k_b z)} \Bigg] . \tag{3.13c}$$

The dc term for each discrete mass is the corresponding continuum mass expression and discreteness causes oscillations in z and X about the continuum value. The terms higher than and including the second harmonic ($n\geq 2$) contribute on the order of a percent or less to the total sum because the coefficients decay exponentially and typically k_b is $O(1)$ or less. Therefore, keeping only the $n=1$ term, we have

$$M_z^d(z,X)=16k_b\left[1+\frac{2k_b z}{\sinh(2k_b z)}\right] + \frac{32k_b\pi}{\sinh(\pi^2/k_b)}\left[\frac{\pi}{k_b}\cos(2\pi z)+\frac{\sin(2\pi z)}{\sinh(2k_b z)}\right]\cos(2\pi X), \tag{3.14a}$$

$$M_X^d(z,X)=16k_b\left[1-\frac{2k_b z}{\sinh(2k_b z)}\right] + \frac{32k_b\pi}{\sinh(\pi^2/k_b)}\left[\frac{\pi}{k_b}\cos(2\pi z)-\frac{\sin(2\pi z)}{\sinh(2k_b z)}\right]\cos(2\pi X). \tag{3.14b}$$

We see from Eq. (3.14) for high-frequency breathers ($k_b\to 0$) that $M_z^d(z,X)\to M_z(z)$ and $M_X^d(z,X)\to M_X(z)$. The continuum values of the masses are recovered in the high-frequency limit. Note that, for a breather, it is the value of k_b and *not* Γ_0 which directly governs whether discreteness effects are large or not. We are assuming, of course, that Γ_0 has not been chosen so small that we are in the "displacive" limit, that is where discreteness effects are essentially eliminated for all values of k_b. For sufficiently large Γ_0 then, our theoretical analysis shows that discreteness effects are negligible in the high-frequency limit which is equivalent to the limit of large subkink width.

We now derive the expression for the total energy $E_{\rm tot}^d$ at $t=0$ for the discrete breather system in the bare approximation by substituting Eqs. (3.14) into Eq. (3.11b) and evaluating the resulting expression at $z=z_0$, the $t=0$ subkink separation, which yields

$$E_{\rm tot}^d(z_0,X)=\tfrac{1}{2}[M_z^d(z_0,X)+M_X^d(z_0,X)] =16k_b\left[1+\frac{2\pi^2/k_b}{\sinh(\pi^2/k_b)}\cos(2\pi z_0)\cos(2\pi X)\right], \tag{3.15a}$$

$$\frac{\Gamma_0}{k_b}\tanh(k_b z_0)=1\ , \tag{3.15b}$$

which is shown in Fig. 2. Equation (3.15a) must be subject to the $t=0$ condition Eq. (3.15b) which, although derived in Sec. II [Eq. (2.16a)] for the continuum case, is valid for the present discrete case because f_l and ϕ_b have the same functional form. Simply put, we are calculating the total energy of a discrete breather at $t=0$ whose subkinks have the same separation as a continuum SG breather at $t=0$. The relationship between the parameters k_b and z_0 for the discrete case is then given by Eq. (3.15b) which is the same as for the continuum case. What has changed for the discrete case is not the relationship between k_b and z_0, but rather the relationship between k_b and ω_b. For discrete SG breathers, the continuum relationship Eq. (2.12) is not true although it is an excellent approximation for high-frequency breathers. For lower-frequency breathers, Eq. (2.12) begins to become inaccurate. For large enough z_0, the Peierls potential pins the breather subkinks (as we will discuss below) and there is no "breathing motion" and one obtains a "static"-breather profile. The relationship Eq. (2.12) then becomes meaningless since ω_b loses its meaning as a breather frequency. In the latter case, the parameters k_b and $\omega_b=(\Gamma_0^2-k_b^2)^{1/2}$ then simply determine the shape of an initial breather profile which does not breathe in the discrete system, but which *would* breathe with a frequency ω_b in the continuum system.

Equation (3.15) is analogous to Eq. (2.16) for the continuum SG breather system. In fact, for high-frequency breathers, Eq. (3.15a) approaches the continuum value $16k_b$. Note in Fig. 2 that the function $E_{\rm tot}^d(z_0)$ cannot be evaluated for arbitrarily small values of z_0 because the condition Eq. (2.21) must be satisfied. Even though we

have calculated the inequality Eq. (2.21) for the continuum SG breather system, we see that it is a high-frequency criterion, which is precisely where discreteness effects are negligible since the breather subkinks have infinite extent. The inequality therefore also holds for the discrete SG breather case.

Figure 2 shows that $E^d_{\rm tot}(z_0)$ is *not* a pure cosine wave in z_0 as Eq. (3.15a) seems to be imply since Eq. (3.15b) must also be satisfied, which changes the value of k_b for each z_0. Consequently, we see that for small z_0 the interaction energy of the subkinks overcomes the effects of the Peierls potential and breathing motion is possible. On the other hand, we see that one does not need z_0 to approach infinity before one obtains "large subkink separation." Actually, only a few kink widths suffice and we can see in Fig. 2 where the breather subkinks will be trapped if started from rest.

Note that the total energy given by Eq. (3.15) is exactly the same as if X were considered a dynamical collective variable. This is because Eq. (3.15) is the energy of $t=0$ breather profiles which are merely *parametrized* by the initial values z_0 and X. Equation (3.15) clearly shows that there exists a Peierls potential for *both* the z_0 and X parameters. In addition, the depth of both Peierls wells are

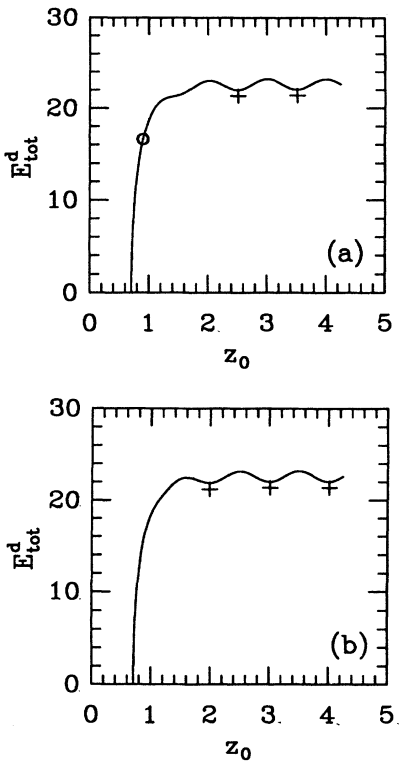

FIG. 2. Total energy as a function of subkink oscillation amplitude z_0, $\Gamma_0=\sqrt{2}$. The solid line corresponds to Eq. (3.15). The center of the plus symbols mark the energies calculated from a static chain and the center of the circle marks the energy of a breather calculated from simulation. (a) $X=0$, (b) $X=\frac{1}{2}$. Since z_0 is measured with respect to X, (a) and (b) each indicate that the minima of the Peierls wells are located between particles.

the same to this order of approximation. For large subkink separation we see that, whether or not the breather is centered on or between particles, the minimum energy is obtained when the subkinks are located between particles. This is in agreement with the results of Ref. 5 in which it was shown that the minimum energy of a single static discrete SG kink is obtained when its center is located midway between particles.

In order to check Eq. (3.15), we have numerically calculated the energies for static-breather profiles such that the breather subkinks are located at the stable Peierls minima near the breather center. For example, for the case $\Gamma_0=\sqrt{2}$, $X=\frac{1}{2}$, we place a continuum breather profile according to Eq. (3.7a) at the center of chain of 3003 particles which are harmonically coupled to their nearest neighbors (spring constant $\mu=1$) and subject the SG potential Eq. (3.7b). We choose $z_0=2.0$ because Fig. 2(b) indicates that a well should be present in this vicinity. We then relax the profile until the maximum force $F_{\rm max}$ on a particle satisfies $F_{\rm max}\leq 10^{-8}\,\mu a$, where $a=1$ is the particle separation in the absence of any kink structures. We measure the static energy according to Eq. (3.1) and determine the relaxed value of z_0 such that the constraint Eq. (3.4a) is satisfied for the resulting relaxed profile. For this case we find $z_0=1.9710$. We repeat the process for cases where the subkinks are trapped in other nearby wells for $X=0$ and $\frac{1}{2}$ and plot the values located by the crosses in Fig. 2.

We must consider the energy scale in order to comment on the agreement. If there are fluctuations in the system such that the subkinks can migrate to the breather center, they will reach zero vacuum energy. The energy scale will then be set by twice the subkink rest mass ($\sim 16\Gamma_0$) and the energies calculated from Eq. (3.15) and from the relaxed chain agree to within 3%. If the temperature is low enough so that the subkinks truly remain trapped, the energy scale is set by the depth of the Peierls potential which then yields a disagreement of about 50%. It has already been shown[7,9] that, when the energy scale is set by the Peierls potential, one must include the q_l for the dressing in order to obtain good quantitative agreement with numerical calculations. Note, however, that the locations of the minima in Fig. 2 from Eq. (3.15) are in good agreement with those computed numerically.

In the case for which z_0 is small enough so that breathing motion results, we show a point (the center of the circle) in Fig. 2(a) corresponding to the total breather energy calculated from simulation for $z_0=0.928$ ($\omega_b=0.868$). We see agreement is good. Discreteness effects are not too large for this case.

We calculate the effective potential for $z(t)$ by considering the equation of motion corresponding to the bare Hamiltonian $H^d_{\rm bare}$ just as we did for the continuum case in Sec. II. The exact equations of motion for the discrete SG breather system are given by Eqs. (3.6a) and (3.6b) into which must be substituted the general expressions for f_l and $V_{\rm SG}(f_l)$ defined in Eq. (3.7). Equation (3.6b) for the z mode (with $q_l=0$) becomes exactly

$$\ddot{z}+\frac{1}{2}\frac{\partial \ln M^d_z}{\partial z}\dot{z}^2=-\frac{1}{M^d_z}\frac{\partial \mathcal{V}^d_{\rm bare}}{\partial z}\,, \tag{3.16}$$

where $\mathcal{V}^d_{\rm bare}$ is given by Eq. (3.8a). As previously explained, we must replace $\mathcal{V}^d_{\rm bare}(z,X)$ in Eq. (3.16) by $V^d_{\rm bare}(z,X)$ which yields

$$\ddot{z}+\frac{1}{2}\frac{\partial \ln M_z^d}{\partial z}\dot{z}^2=-\frac{1}{M_z^d}\frac{\partial V^d_{\rm bare}}{\partial z} \ . \tag{3.17}$$

We see that Eq. (3.17) is of the same form as Eq. (2.18) for the continuum case and that the general potential for z depends on the square of the velocity $\dot{z}^2$ as in the continuum case.

We treat the velocity effects on the potential in Eq. (3.17) by considering the expression for the total energy from Eq. (3.11):

$$\tfrac{1}{2}M_z^d(z,X)\dot{z}^2+V^d_{\rm bare}(z,X)=E^d_{\rm tot} \ , \tag{3.18a}$$

which we rewrite as

$$\tfrac{1}{2}\dot{z}^2+V^d_{\rm eff}(z,X)=0 \ , \tag{3.18b}$$

where

$$V^d_{\rm eff}\equiv\frac{1}{M_z^d(z,X)}[V^d_{\rm bare}(z,X)-E^d_{\rm tot}] \ , \tag{3.18c}$$

where $E^d_{\rm tot}$ is given by Eq. (3.15). The time derivative of Eq. (3.18b) yields the simple equation of motion

$$\ddot{z}=-\frac{\partial V^d_{\rm eff}(z,X)}{\partial z} \tag{3.19}$$

which is equivalent to Eq. (3.17).

The potential $V^d_{\rm eff}(z,X)$ is shown in Fig. 3. We see there exists a large central well representing the attractive force between the subkinks when they are close to each other and oscillations at larger subkink separation representing the Peierls potential. The effects of the Peierls potential are diminished in the vicinity of the central well. Consequently, if the breather subkinks are oscillating sufficiently near the bottom of the central well, discreteness effects are small and we have $M_z^d(z,X)\to M_z(z)$, $M_X^d(z,X)\to M_z(z)$ and Eq. (3.17) reduces to Eq. (2.18).

We measure the instantaneous potential energy for a SG breather as a function of $z(t)$ from simulation in order to compare with the collective-variable theory. We choose an initial breather profile such that the subkinks will not be trapped when started from rest and let the motion evolve according to the discrete SG equation given by Eqs. (3.2) and (3.7b). As the motion evolves, we measure the potential energy at various times according to the potential part of the Hamiltonian in Eq. (3.1). We determine the value of $z(t)$ for the instantaneous profile at time t by requiring the constraint Eq. (3.4a) to be satisfied. Since we are measuring the potential energy directly, it is correct to compare with $V^d_{\rm bare}(z,X)$ given by Eq. (3.11b) rather than with the rescaled effective potential $V^d_{\rm eff}$ in Eq. (3.18c). We show the comparison in Fig. 3(c). The only discrepancies come from the region of the turning points of the oscillation where discreteness effects are becoming more significant.

For completeness, we note that if the subkinks are separated by large z, $\tanh(k_b z)\to 1$ and Eq. (3.6b) with $q_2=0$ reduces to

$$\ddot{z}+\frac{1}{2}\frac{\partial \ln M_z^d}{\partial z}\dot{z}^2=\frac{2}{4!M_z^d}\langle f_l'|f_l'''\rangle \ . \tag{3.20}$$

Equation (3.20) is exactly the discrete bare equation of motion for the center of mass of a single SG kink derived in Ref. 6. The fourth derivative term comes from considering the quantity $\Delta_2 f_l$ in Eq. (3.6b) expanding it in a Taylor series and keeping only the first two terms the first of which cancels the last term in Eq. (3.6b). Equation (3.20) describes the dynamics of the breather subkinks when they are sufficiently separated so that they do not interact.

C. Small oscillations about a static-breather profile

If the breather subkinks are trapped then we have a quasistatic-breather profile to which we assign the equilibrium values z_0 and X_0. We expect that the small-oscillation frequency spectrum about such a profile will

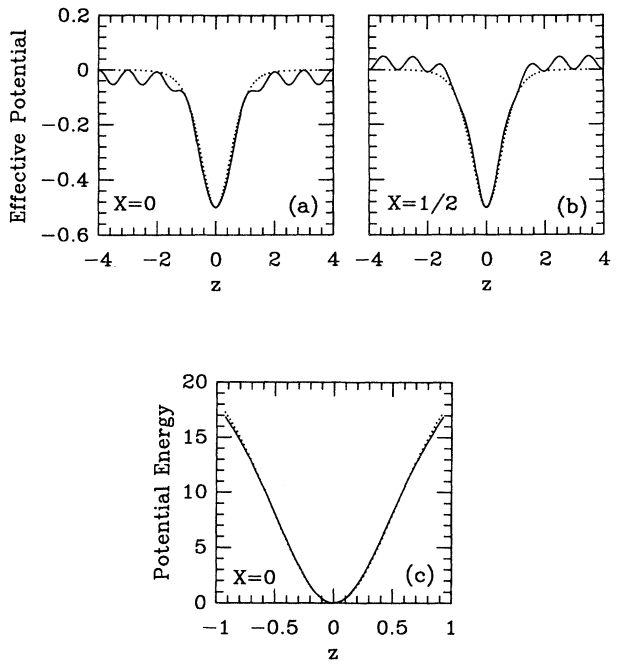

FIG. 3. $\Gamma_0=\sqrt{2}$. In (a) and (b) are shown the effective potentials for the collective variable z for $X=0$ and $\frac{1}{2}$, respectively. The solid line corresponds to Eq. (3.18c) and the dotted line to the continuum, Eq. (2.19c). (c) The solid line shows the instantaneous bare potential for a discrete breather calculated from simulation for $\Gamma_0=\sqrt{2}$, $X=0$. We treated the phonon contribution of the potential energy, which is about 1% of the total potential energy, as a simple dc shift that originally appeared on the solid line in (c) and simply subtracted it out of the data; therefore, the solid line now touches the $z(t)$ axis. The dotted line corresponds to Eq. (3.11b) where we used the simulation value $z_0=0.9282$ and the corresponding value $k_b=1.0767$ from Eq. (3.15b). The observed frequency is $w_b^{\rm sim}=0.8679$. We have not derived a formula which gives the frequency of a discrete breather (see end of Sec. V).

consist of an in-phase mode of the subkinks corresponding to the oscillatory center-of-mass motion $X(t)$ of the breather about the equilibrium value X_0 (where we must now allow X to become time dependent), an out-of-phase mode corresponding to the z motion about the value z_0, and the phonon states. If the separation between the trapped subkinks is large, then the subkinks essentially do not interact, the frequencies of the in-phase and out-of-phase modes are degenerate and the problem of trapping reduces to that of the dynamics of a single discrete SG kink, which has already received much attention. However, if the subkinks are trapped, say, in the first Peierls wells which appear on either side of the central well, then the interaction of the subkinks is nonnegligible and we expect that the in-phase and out-of-phase frequency line will be split into a doublet.

The lower frequency of the doublet corresponds to the internal z mode and *not* the center-of-mass X mode. We show this by examining a small displacement of the static-breather profile for each collective mode which is shown in Fig. 4. Figure 4(a) shows that the center-of-mass mode corresponding to a small shift of the subkinks in the same direction has a node at the center of the eigenfunction. For a small shift of the subkinks in opposite directions, Fig. 4(b) shows that the z-mode eigenfunction has no node. Therefore, the center-of-mass mode corresponds to the higher frequency whereas the z mode corresponds to the lower frequency.

It is apparent that the higher frequency of the doublet is associated with the center-of-mass mode because the two subkinks are antiparticles of one another, i.e., they have opposite helicities. If we were considering the small-oscillation spectrum of two trapped *kinks* which have the same helicity (as for a pinned discrete double sine-Gordon profile), then a similar inspection of the eigenfunctions shows that the in-phase mode has the lower frequency and the out-of-phase mode the higher frequency. Another way of looking at this phenomenon is to note that the masses associated with the two modes are not the same, $M_z^d > M_X^d$. Thus, the internal z mode associated with M_z^d corresponds to the lower frequency if the increase in mass from M_X^d to M_z^d is enough to overcompensate for the increase in the effective force constant. We see that this is indeed the case from the following calculation where we derive expressions for the frequencies of the doublet and then evaluate the expressions numerically.

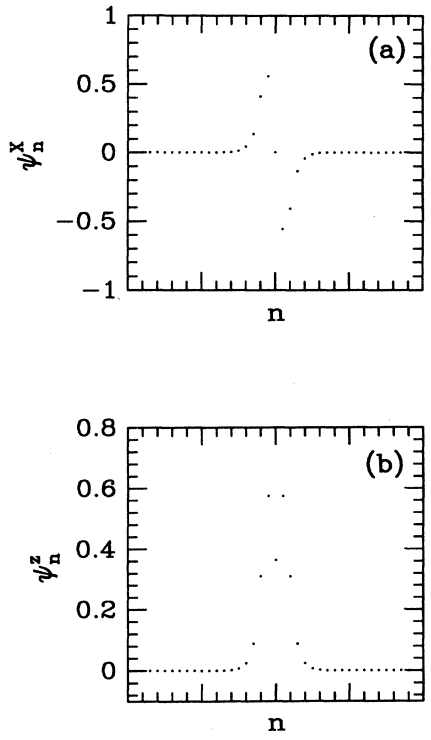

FIG. 4. (a) Center of mass and (b) internal mode eigenfunctions about a "static"-breather profile for $\Gamma_0=\pi/2$, $X=0$.

It is possible to calculate a closed-form expression for the frequency of the z mode using Eq. (3.18) but unfortunately the expression is too large to be of any use. We therefore derive expressions for the frequencies of the doublet in a different manner[33(a)] which incorporates the exact shape of the metastable static-breather profile and which, at the same time, relates collective variable theory for the small-oscillation problem to standard perturbation analysis. The formulas we now derive for the frequencies of the doublet are valid for any kink width but they must be evaluated numerically.

Since we seek an expression for the frequency of the X mode as well as the z mode, we must necessarily promote X from a fixed parameter to a time-dependent collective variable $X(t)$ in addition to $z(t)$ and we therefore need to introduce an ansatz and a total of four constraints. We denote the exact static-breather profile by $\hat{f}_l(z_0,X_0)$. In general, the function $\hat{f}_l(z,X)$ represents a departure of the breather profile from the exact stable state. Two of the constraints are given by Eqs. (3.4a) and (3.4b) with the replacement $f_l \rightarrow \hat{f}_l(z,X)$ and the other two are

$$C_3=\langle \partial \hat{f}_l(z,X)/\partial X|q_l\rangle=0$$

and

$$C_4=\langle \partial \hat{f}_l(z,X)/\partial X|p_l\rangle=0 .$$

In order to construct the ansatz, we first substitute

$$Q_l=\hat{f}_l(z_0,X_0)+\epsilon \exp(-i\omega_m t)\psi_l^m$$

into the discrete SG equation of motion

$$\ddot{Q}_l-\Delta_2 Q_l+\Gamma_0^2 \sin Q_l=0 \tag{3.21}$$

and linearize in the small parameter ϵ to obtain the eigenvalue equation

$$\mathcal{L}\psi_l^m=\omega_m^2\psi_l^m-\alpha_m(z,X)\psi_l^m , \tag{3.22a}$$

where m labels the mth eigenstate. That is, ψ_l^m represents ψ_l^X, ψ_l^z, or ψ_l^k for the kth phonon state. The operator $\mathcal{L}$ is defined by

$$\mathcal{L}\equiv-\Delta_2+\Gamma_0^2\cos[\hat{f}_l(z_0,X_0)] . \tag{3.22b}$$

We have also included in Eq. (3.22a) a Lagrange multiplier $\alpha_m(z,X)$ which constrains the profile at an arbitrary z or X thus introducing z and X dependence into the

eigenfunctions ψ_l^m. Therefore, $\alpha_m(z_0,X_0)=0$ since there is no constraint needed to keep the system at equilibrium.

We choose the ansatz which depends on the eigenfunctions ψ_l^m of the operator $\mathcal{L}$ in the following way:

$$\begin{aligned} Q_l &= \hat{f}_l(z,X)+q_l \\ &= \hat{f}_l(z_0,X_0)+\int_{X_0}^{X}\psi_l^X(z_0,X')dX' \\ &\quad +\int_{z_0}^{z}\psi_l^z(z',X_0)dz'+q_l \ , \end{aligned} \tag{3.23}$$

which will make the connection between collective-variable theory and the standard perturbation analysis. Since the ansatz function $\hat{f}_l(z,X)$ takes into account all static discrete effects, the q_l in Eq. (3.23) represent only the radiated phonons which are zero in the limit of small oscillations about the exact profile $\hat{f}_l(z_0,X_0)$. The constraints are therefore identically satisfied.

Substituting Eq. (3.23) into Eq. (3.21) and linearizing in z and X, we obtain

$$\psi_l^z(z_0,X_0)\ddot{z}+\psi_l^X(z_0,X_0)\ddot{X}+\mathcal{L}[\psi_l^z(z_0,X_0)(z-z_0)+\psi_l^X(z_0,X_0)(X-X_0)]=0 \ . \tag{3.24}$$

Projecting Eq. (3.24) in the direction $\psi_l^z(z_0,X_0)$ and solving for $\ddot{z}$, we obtain

$$\ddot{z}=-\left.\frac{\langle\psi_l^z|\mathcal{L}|\psi_l^z\rangle}{\langle\psi_l^z|\psi_l^z\rangle}\right|_{z_0,X_0}(z-z_0) \ . \tag{3.25a}$$

Projecting Eq. (3.24) in the direction $\psi_l^X(z_0,X_0)$ and solving for $\ddot{X}$, we obtain

$$\ddot{X}=-\left.\frac{\langle\psi_l^X|\mathcal{L}|\psi_l^X\rangle}{\langle\psi_l^X|\psi_l^X\rangle}\right|_{z_0,X_0}(X-X_0) \ . \tag{3.25b}$$

In deriving Eqs. (3.25) we used the orthogonality condition

$$\langle\psi_l^z(z_0,X_0)|\psi_l^X(z_0,X_0)\rangle=0 \ . \tag{3.26}$$

From Eqs. (3.22a) and (3.25) we see that the frequencies of the doublet are given by

$$\ddot{z}=-\omega_z^2(z-z_0), \quad \ddot{X}=-\omega_X^2(X-X_0) \ , \tag{3.27a}$$

$$\begin{aligned} \omega_z^2 &= \left.\frac{\langle\psi_l^z|\mathcal{L}|\psi_l^z\rangle}{\langle\psi_l^z|\psi_l^z\rangle}\right|_{z_0,X_0} \\ \omega_X^2 &= \left.\frac{\langle\psi_l^X|\mathcal{L}|\psi_l^X\rangle}{\langle\psi_l^X|\psi_l^X\rangle}\right|_{z_0,X_0} . \end{aligned} \tag{3.27b}$$

Therefore, when we use the ansatz Eq. (3.23) we have the result that the frequencies of the doublet in the collective-variable theory Eq. (3.27a) are given by the eigenvalues of Eq. (3.22a) with $\alpha_n(z_0,X_0)=0$ and necessarily yield agreement with simulation.

We compare Eq. (3.27) with results calculated from simulation for the case $\Gamma_0=\pi/2$. The spectrum is determined from simulation by relaxing an initial condition as described in the previous subsection to generate a stable static-breather solution. The solution is given random noise of amplitude $\sim 10^{-4}\,a$ and we analyze the resulting dynamics of Eq. (3.21) by calculating the Fourier transform of the motion of one particle in the quasistatic breather.

Let us first consider $z_0=1.4498$ which is the smallest value of z_0 that leads to a static breather for our choice $\Gamma_0=\pi/2$. The relaxed profile $\hat{f}_l(z_0,X_0)$ is centered on a particle. The Fourier spectrum shown in Fig. 5(a) consists of two large peaks with frequencies $\omega_z^{\rm sim}=0.763\pm0.006$ and $\omega_X^{\rm sim}=1.013\pm0.006$. We obtain from Eqs. (3.22a) and (3.27) the values $\omega_z=0.759$ and $\omega_X=1.01$. We see agreement is excellent because of the choice of the ansatz Eq. (3.23). In addition, we notice in Fig. 5 that the phonon band is in the approximate frequency range $1.5\le\omega\le2.5$ which is consistent with the frequency values calculated from the discrete dispersion law

$$\omega^2(k)=4\sin^2\left[\frac{k}{2}\right]+\Gamma_0^2 \ , \tag{3.28}$$

which are $\omega(0)=\Gamma_0\approx1.57$ and

$$\omega(\pi)=(\Gamma_0^2+4)^{1/2}\approx2.54 \ .$$

In order to calculate the phonon modes using collective-variable theory, we must use Eq. (3.6a) for the q_l, but this is not one of the goals of the present paper.

Figures 5(b)–5(e) show similar Fourier transforms for which the breather subkinks are trapped in wells that are progressively further apart. We see the gradual decrease in the line splitting with increasing z_0. The last panel, Fig. 5(f), shows the doublet frequencies as a function of z_0. Note that the upper frequency of the doublet reaches a maximum at $z_0=1.9916$, whereas there is no such maximum for the lower frequency.

IV. MOLECULAR-DYNAMICS SIMULATIONS FOR DISCRETE SG BREATHERS

A. Frequency spectrum

In this section we are interested in a discrete breather whose subkinks are no longer trapped in the Peierls potential and want to investigate particularly (a) its stability depending on its location with respect to the lattice sites and (b) its lifetime. Our analysis is based upon the numerical simulation of the dynamics of the breather and the investigation of the waves that it radiates.

Let us illustrate the method by one example for $\Gamma_0=\sqrt{2}$ and $\omega_b(t=0)=1$ which corresponds to a moderately discrete breather. The initial condition is a continuum profile with $z_0\approx0.88$ situated at the position

$X=1500.5$ in a chain of 3003 particles. When the system evolves according to Eq. (3.21), this initial state, which is not a solution for the discrete system, first shows a fast transient during the first few oscillations after which the breather frequency is $\omega_b^{\rm sim}=0.959\pm0.006$, slightly less than the initial condition. Then the solution shows a virtually constant amplitude of oscillation accompanied by an extremely weak emission of radiation. In order to analyze this radiation, we calculate the magnitude of the temporal Fourier transform $|\mathcal{F}[Q_l(t)]|$ of the motion for each of the 100 center particles of the chain which contain the breather. We construct a matrix of frequency versus particle number thereby forming relief of the transform and normalize the largest peak in the matrix to unity. Choosing a cutoff between 0 and 1, we plot a point for each peak in the relief matrix whose magnitude exceeds the cutoff value. The duration of the transform is approximately 160 breather oscillations and is started after the initial transient effects have radiated away. The results are shown in Fig. 6(a) which corresponds to a cutoff of 1.5×10^{-4}. The cutoff is chosen just above the noise level. Figure 6(b) shows the relative amplitudes of the Fourier transform for a particle inside the breather. The value $\omega=3$ represents the Nyquist frequency—the highest sampled frequency—for all our simulations.

We see there exists spatially localized and nonlocalized states in Fig. 6(a). We first focus our attention on the nonlocalized states of which there are six and as we might expect they are situated inside the phonon band. The lowest nonlocalized state is the lower phonon band edge which has a measured frequency $\Gamma_0^{\rm sim}=1.417\pm0.006$ which agrees with $\Gamma_0=\sqrt{2}$ within the frequency resolution. The lower band edge in Fig. 6(a) is pronounced because there is some relaxation of the inexact initial condition and the phonons created at these frequencies cannot propagate away because they are standing waves, or at least nearly so, with small group velocities. They are therefore present throughout the duration of the transform. Campbell *et al.*[15] call this "prompt" radiation. The other five pronounced phonon states in Fig. 6(a) arise because of spatially localized modes (whose origin we discuss below) associated with the breather which are present in the phonon band at these specific frequencies and excite phonons. What appears to be the upper band edge in the simulation of Fig. 6(a) is actually a phonon excited by a localized mode whose frequency is just below the upper edge.

Now we consider the localized states in Fig. 6(a). They are outside of the phonon band as expected. We find the frequency of the largest (in space) localized state is $\omega_b^{\rm sim}=0.959\pm0.006$, which we associate with the fundamental frequency of the breather oscillation. The breather mode looks rather extended in space and this is merely because the cutoff is such that we see those particles

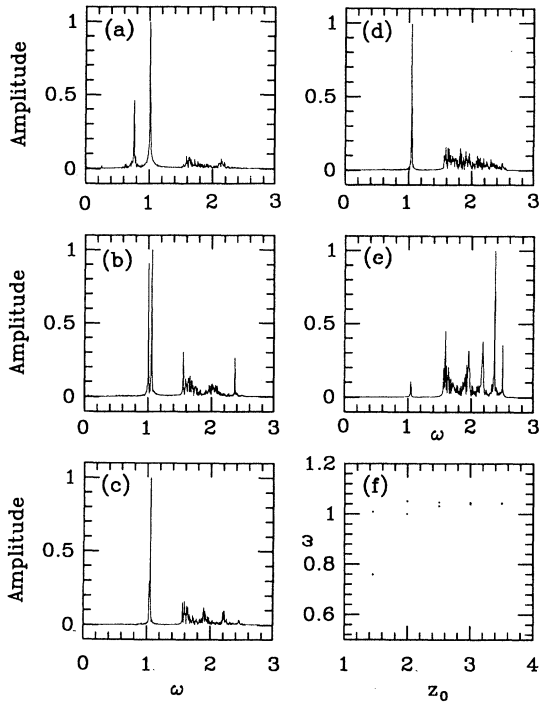

FIG. 5. Fourier transform of a particle during small oscillations about a "static"-breather profile for $\Gamma_0=\pi/2$. Parameter values are $(z_0, X \bmod n)$=(a) (1.4498,0), (b) (1.9916,$\frac{1}{2}$), (c) (2.4979,0), (d) (2.9994,$\frac{1}{2}$), (e) (3.4998,0), where n is an integer. (f) shows the frequencies of the doublet as a function of equilibrium value z_0. Note that a maximum exists for the center-of-mass mode (upper sequence of dots) but does not exist for the internal mode.

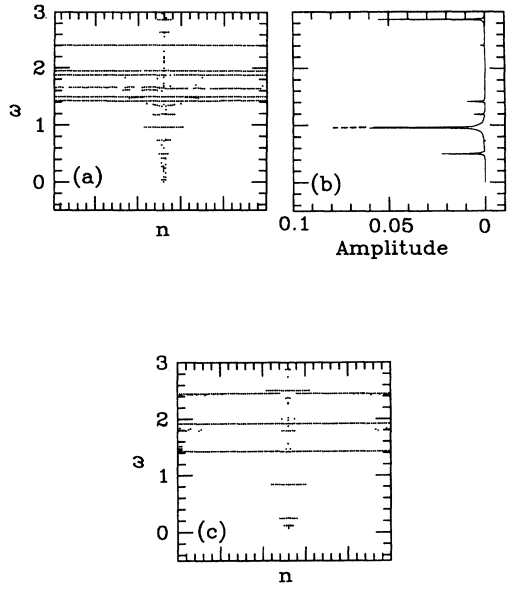

FIG. 6. (a) Frequency vs particle number for $\omega_b=0.959\pm0.006$, $\Gamma_0=\sqrt{2}$, $X=0$. (b) shows the relative amplitude vs frequency of the states in (a) for a particle in the breather and has been turned on its side for easy comparison with (a). The largest peak in (b) corresponding to the breather frequency is normalized to unity indicated by the dotted line. All other peaks show actual amplitudes. (c) shows the frequency vs particle number for $\omega_b=0.837\pm0.006$, $\Gamma_0=\sqrt{2}$, $X=0$. The nonlocalized state of highest frequency appearing in (a) is not the upper band edge, but it is the upper band edge in (c).

whose amplitudes of oscillation are at least 0.015% of the largest amplitude in the system which is the breather mode. Some other localized states can be identified because they correspond to breather harmonics but we must recall that only odd multiples of the breather frequency will be present for our case due to the symmetry of the underlying potential. We call the breather the first harmonic. Although there is a frequency in the phonon band that appears to be resonating at $2\omega_b^{\rm sim}$, a quantitative check shows that this is not the case. Its origin will be discussed below. The third harmonic which has a frequency $(3\omega_b)^{\rm sim}=2.864\pm0.006$ is directly seen in Fig. 6(a) and corresponds to the second largest peak in Fig. 6(b). The fifth harmonic cannot be observed directly because it exceeds the Nyquist frequency of our transform, but its presence is observed indirectly since it has been aliased (folded back) into the range of sampled frequencies $\omega<3$ by the discrete transform and appears at $(5\omega_b)^{\rm sim}\rightarrow1.185\pm0.006$ just above the breather mode. The understanding of the other localized states is less simple. In particular, the two modes that *appear* to be first and second subharmonics ($\sim\omega_b/2$ and $\sim\omega_b/4$) do not coincide exactly with these values. Figure 6(c) clearly shows for the case $\omega_b=0.837\pm0.006$ that the subharmonics are not present.

The origin of the local and nonlocal states not yet identified can be determined by observing their evolution in a series of numerical simulations for various breather frequencies in the range $0.837\leq\omega_b\leq1.406$. This frequency range is natural for our choice of $\Gamma_0=\sqrt{2}$ since it insures that the breather frequency is always in the gap below the lower band edge while at the same time the third harmonic lies above the upper band edge. This criterion corresponds to a long breather lifetime and makes an accurate Fourier transform possible, as we will discuss in detail in Sec. IV C.

All our simulations in the above frequency range use breathers centered on particles. For each simulation we construct a plot analogous to Fig. 6(a) but which has a cutoff value equal to zero in order to observe all possible structures. Although there is some noise seen when using very low cutoff values, many low-amplitude modes can still be clearly identified. We record the frequencies of all the prominent states (both spatially localized and nonlocalized) and present these prominent frequencies as a function of breather frequency in Fig. 7 where we have connected the points by lines in such a way that the same states, from case to case, are identified. We determined which states were the same by inspecting their signatures from figures like 6(a). Some of the points in Fig. 7 do not have a line drawn through them. Such points correspond to states, say, that were seen in just one of the 22 simulations. The two horizontal lines in Fig. 7 locate the phonon band edges which are the same for all the simulations since $\Gamma_0=\sqrt{2}$ for each case.

First consider only the states represented by solid circles which converge to a point on the lower band edge. The frequency difference between all the lines connecting these states is clearly defined by the frequency difference between ω_b and the lower phonon band edge. These states are just the combination modes obtained by expanding the sine term in the SG equation and considering the odd powers of

$$S=[\exp(i\omega_b t)+\exp(i\Gamma_0 t)]+\text{c.c.}\ ,$$

from which all the frequencies for these states are reproduced. The complex conjugate part accounts for the solid lines of negative slope, including the one that seems to be "reflected" at the value $\omega=0$. Figure 7 clearly shows that there is no pattern for subharmonics of ω_b, even though Fig. 7 was constructed from frequency spectra like Fig. 6(a), but with a cutoff value equal to zero.

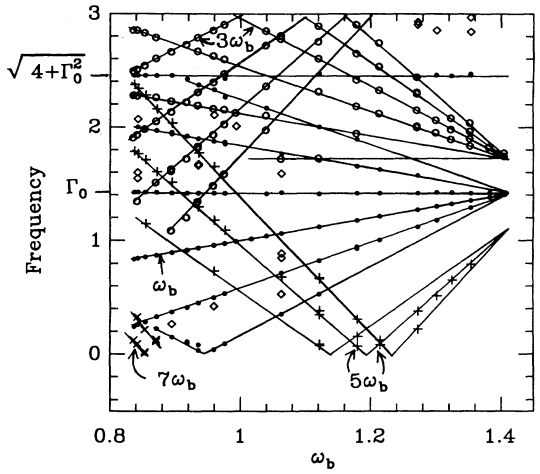

FIG. 7. Most prominent states in the discrete-breather frequency spectrum as a function of breather frequency. The symbols represent the combination modes for the following states: (●) breather frequency, (○) third harmonic, (+) fifth harmonic, (×) seventh harmonic, and (◇) modes which appear to be unique to a single case. We also used (●) to represent the band edges. The abcissas in Fig. 7 are obtained from the Fourier-transform results and do not correspond to the $t=0$ choice of the parameter ω_b. For some cases the value of the breather frequency decreases slightly from the initial value and for other cases it increases.

We introduce the convenient notation $C(\omega_1,\omega_2)$ in order to represent the set of frequencies corresponding to all combination modes between two arbitrary states ω_1 and ω_2. Then, just as the solid circles represent the combination modes $C(\omega_b,\Gamma_0)$, the open circles represent the combination modes $C[3\omega_b,C(\omega_b,\Gamma_0)]$; that is, they are associated with the third harmonic. The Nyquist frequency accounts for the apparent "reflection" of the lines at the "boundary" $\omega=3$. These frequencies have simply been aliased back into the range $\omega\leq3$ by the discrete Fourier transform. If the Nyquist frequency was chosen sufficiently larger, the states represented by the open circles would not be reflected and would converge to a point above $\omega=3$ instead of where they converge in Fig. 7.

In a similar fashion, the states denoted by plus signs are combination modes related to the fifth harmonic. They have also been aliased back into the range $\omega_b\leq3$ by the choice of Nyquist frequency. Again, the complex conjugate accounts for their apparent reflection at the value $\omega=0$. The x's, which lie in the lower left-hand

corner, correspond to the seventh harmonic.

Some points in Fig. 7 which do not lie on a line represented by the diamonds seem to be accounted for if we consider combination modes involving the phonon at the upper band edge. The remaining unidentified points likely involve more complicated combination modes. Thus, all the points in Fig. 7 seem to be accounted for by more or less complicated frequency combinations involving the breather frequency, its odd harmonics, and the phonon band edges which have been excited by the inexact initial conditions and which persist throughout the simulation because of their nearly zero group velocity. The generality of the existence of the combination modes, which is to be expected via the nonlinearity, is easily checked by exciting a phonon at an arbitrary frequency. We have done so and observed the proper combination modes in the resulting frequency spectrum.

As a final remark, we note that, since the excitation of the band edges is unavoidable, Fig. 7 represents, in some sense, a fundamental portrait of the discrete SG breather spectrum.

B. Stability of breather's center of mass

We noted in the previous subsection that our simulations use breathers centered on particles for the choice $\Gamma_0=\sqrt{2}$. All breathers centered between particles throughout the above frequency range $0.837 \leq \omega_b \leq 1.406$ are unstable in X—the breather center of mass moves. Breathers centered on a particle are stable in X *except* in the approximate subrange $0.993 \leq \omega_b \leq 1.040$, where the center of mass of the breather moves. Therefore, in this frequency subrange neither breathers centered on particles or between particles are stable in X. (Most modes in the Fourier transform for the frequency subrange $0.993 \leq \omega_b \leq 1.040$ are smeared in frequency except for very strong modes, like the breather and its third harmonic.)

We can obtain a partial theoretical understanding of the breather's X stability based on Eq. (3.15a) from which we find

$$\mathrm{sgn}[E^d_{\mathrm{tot}}(X=0)-E^d_{\mathrm{tot}}(X=\tfrac{1}{2})]=\mathrm{sgn}[\cos(2\pi z_0)]\ , \qquad (4.1)$$

where the signum function sgn means "sign thereof." To this order of approximation, the stability oscillates between $X=0$ and $\frac{1}{2}$ and is determined by the magnitude of z_0. Since we have chosen $\Gamma_0=\sqrt{2}$, we must have $z_0 \geq 1/\sqrt{2}$ by Eq. (2.21). Equation (4.1) indicates that, for $1/\sqrt{2} < z_0 < 1$ ($1.29 < \omega_b < \sqrt{2}$), breathers centered on particles are stable which agrees with our simulations. However, for slightly lower frequencies than $\omega_b = 1.29$, the stability predicted by Eq. (4.1) shifts to $X=\frac{1}{2}$ which is in disagreement with our observations. However, as the frequency becomes still lower, or as the amplitude z_0 becomes larger $z_0 \geq 2$, we obtain agreement again, which corresponds to the static-breather case. That is, the breather subkinks for larger z_0 will be trapped and Eq. (4.1) predicts correctly whether the static-breather center will be located on or between particles for a given z_0.

Therefore, Eq. (4.1) is in agreement for high-frequency breathers and low-frequency breather profiles which result in static-breather configurations. On the other hand, Eq. (4.1) disagrees with simulation for cases in which the subkink interaction energy at separation z_0 is comparable with the depth of the Peierls wells. In this latter z_0 range, the prediction of the stability of the X motion seems to be very sensitive to approximations made on the collective-variable equations of motion, such as neglecting the q_l dressing, even for moderately high frequencies. For instance, the potentials from theory and simulation in Fig. 3(c) for $\omega_b \approx 0.9$ seem to be very close, yet the stability prediction for the X motion for the same ω_b is incorrect.

We also note a general property of Eq. (4.1) which is that it always predicts a stable configuration to be at $X=0$ *or* $\frac{1}{2}$. Thus, it can never predict (to this order of approximation) the observed result of instability for $X=0$ *and* $\frac{1}{2}$. We have not probed why both symmetry values for X were unstable in the subrange $0.993 \leq \omega_b \leq 1.040$ in the simulations.

C. Breather lifetime

If we consider a moderately low-frequency breather and choose the parameters $\Gamma_0=\sqrt{2}$ and $\omega_b(t=0)=0.3$, the third harmonic lies initially below the phonon band and the fifth harmonic lies in the band and resonates with the phonons thereby radiating energy. Since energy is conserved, the breather amplitude must decrease thereby increasing the frequency. The breather frequency $\omega_b(t)$ is thus a strongly dependent function of time. Consequently, the harmonics of $\omega_b(t)$ all increase in frequency. The third harmonic eventually passes into the band by crossing over the lower phonon and edge and the radiation rate increases. The breather continues to radiate phonons and $\omega_b(t)$ continues to increase with time until the third harmonic passes out of the band by crossing over the upper phonon band edge. The radiation rate then decreases drastically. Measurements of the breather frequency calculated over individual cycles during the simulation show that $(3\omega_b)^{\mathrm{sim}}$ has migrated from below the phonon band to the upper band edge after only six breather oscillations at which time the breather frequency obtains the critical value $w^{\mathrm{sim}}_{\mathrm{crit}}=0.818\pm0.006$ which remains constant for the remainder of the simulation (about 150 breather oscillations). This is a *remarkably* sharp transition from short breather lifetime to long breather lifetime. The sharpness of the transition is still observed if we start with a profile corresponding to the $t=0$ parameter $\omega_b=0.75$ so that the third harmonic is in the band and not far from the upper edge, the difference being $\Delta\omega \approx 0.2$. We observe that the harmonic rises in frequency and, in five breather oscillations, reaches exactly the same critical frequency as in the previous case, which remains constant for the remainder of the simulation. The sharpness of the transition is therefore independent of the initial breather frequency. After the third harmonic crosses over the upper phonon band edge, the only states resonating with phonons are the combination modes whose effects are very weak.

Figure 8 shows the Poynting's flux of radiation calcu-

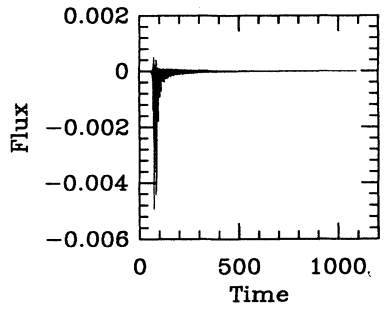

FIG. 8. Instantaneous Poynting's flux of phonon radiation calculated 30 particles away from breather center corresponding to the $t=0$ condition $w_b=0.3$. After six breather oscillations, $(3\omega_b)^{\text{sim}}$ crosses over the upper phonon band edge.

lated from the simulation for the former case. The flux does not show the sharpness of the transition because many of the phonons initially radiated by the breather are long wavelength and take a long time to reach the "flux detector" which is 30 particles from the breather center. Thus, the signature of the transition is smeared out in Fig. 8. Nevertheless, we estimate the lifetime of the breather by noting that the energy flux at the end of the simulation in Fig. 8 averages to $\langle P\rangle\approx 10^{-6}$. Using $\omega_b=0.818$ (period $T_b=7.68$) and $k_b=1.15$ (energy $E\approx 16k_b=18.4$), we find that, during one oscillation, the breather loses

$$\Delta E/E=T_b\langle P\rangle/E\approx 4\times 10^{-3}\%$$

of its energy. Assuming that, as the breather decays it loses this percentage of its energy after each oscillation, we *under*estimate that the lifetime of the breather is on the order of some tens of thousands of oscillations, about four orders of magnitude greater than the lifetime before the transition. It is now apparent why we required the third harmonic to lie above the phonon band when calculating the temporal Fourier transform of the breather dynamics in the previous subsection.

Notwithstanding its long lifetime, our simulations suggest that a SG breather is not stable as $t\to\infty$ even if the third harmonic is above the phonon band. There are still combination modes in the band which excite phonons and their effects are small but not zero. A complete elimination of the band-edge phonons would imply an exact discrete breather solution since the combination modes would be completely eliminated and no phonons would be radiated and this is not a possibility. However, if we could at least reduce the amplitude of phonons at the band edges in the simulation, we would perhaps be able to find a discrete breather solution that is even "more" stable (longer lifetime) than the ones considered above since that would reduce the amplitude of the combination modes in the band. However, reducing the number of band-edge phonons is extremely difficult since the excitation at the band edges is a long-time effect of arbitrary initial conditions.[15] Consider the crude example of running a simulation for some time after which phonons are observed on the chain which have been radiated by the breather. Now suppose we set the phonons to zero by hand in order to obtain a more stable discrete breather solution. This is easy to do *away* from the breather, but in the vicinity of the breather it is virtually impossible because one does not known how much of the discrete field is "breather" and how much is "phonons." It is a time-dependent state. Band-edge phonons not set to zero in the breather vicinity will spread, lower their amplitude, but still be present. Although such a process may yield discrete breathers with longer lifetimes, we have not tried it.

Another possibility for finding highly stable breather solutions in discrete systems is to consider very short systems—less than 100 particles. The phonon spectrum is then "very" discrete. If all combination modes between the breather, its harmonics, and all phonons are such that the combination modes in the band lie *in between* the phonon states, then the discrete breather solution will have an infinite lifetime since the radiation will decay exponentially with a positive imaginary wave number. Recent work for the ϕ^4 model shows that such stable discrete breather solutions exist.[36]

We conclude from molecular-dynamics simulations that breather frequencies such that the third harmonic is above the phonon band are "highly" stable. This numerical observation based on Fourier analysis complements the theoretical result that discreteness effects are less important in high-frequency breathers. In addition, however, the numerical analysis gives a precise criterion for deciding whether the breather frequency is high enough for discreteness effects to be considered negligible. We must have

$$\omega_b>\tfrac{1}{3}(4+\Gamma_0^2)^{1/2}\,, \tag{4.2a}$$

where the right-hand side is one-third of the frequency of the upper phonon band edge. Equation (4.2a) corresponds to a critical amplitude of oscillation

$$z_c=\frac{3}{2(2\Gamma_0^2-1)^{1/2}}\tanh^{-1}\left[\frac{2}{3\Gamma_0}(2\Gamma_0^2-1)^{1/2}\right], \tag{4.2b}$$

where we made use of Eq. (3.15b). Then the only states resonating with phonon modes will be combination modes whose effects are very weak. Note that, for values $\Gamma_0^2\le\frac{1}{2}$, Eq. (4.2b) predicts that the value z_c does not exist. This is because the third harmonic of ω_b will never be above the upper band edge. On the other hand, smaller Γ_0 implies a smaller upper limit on k_b than in the cases considered above and hence for small enough Γ_0 we will be in the displacive limit and discreteness effects will be small for all allowed values of k_b.

V. DISCUSSION AND CONCLUSION

We have employed collective-variable theory and molecular-dynamics simulations in order to study the statics and dynamics of breather excitations in the center-of-mass frame in one-dimensional continuum and discrete systems. We derived the exact collective variable equations of motion for $z(t)$ and the coupled phonon field for continuum and discrete systems and applied the

theories to the SG case.

The complete integrability of the continuum SG case in a collective-variable context leads to the interesting result that the slopes of the colliding subkinks are exactly constant which is true for any exact two-soliton collision, not just the breather. The standard relativistic mass dilation due to the change in velocity near the collision region is balanced exactly by the change in the local effective potential acting on the subkinks because the subkink masses depend on the value of the local potential relative to the vacuum. It is likely that this mass constancy also exists for an exact N-soliton solution due to the exact integrability leading and the absence of phonons. The continuum theory also serves as a useful reference for comparing the theoretical results of the discrete SG case.

The calculations for the discrete case show that there exist three regimes of breather motion. One regime corresponds to high-enough-frequency breathers which can oscillate such that the interaction energy between the subkinks at maximum separation z_0 is sufficiently greater than the depth of the Peierls wells. The bare theory agrees well with this case since discreteness effects are not too large. A second regime corresponds to the opposite case where the breather subkinks are situated far enough apart so that the interaction energy is sufficiently weak,the subkinks are trapped by the Peierls wells, and a "static"-breather profile results. The bare theory gives acceptable results (to within 3%) for the energy of such a state if the energy scale is governed by twice the subkink rest mass, but if the scale is set by the depth of the Peierls well we need to incorporate the dressing into the theory in order to calculate meaningful numbers. We have taken into account the exact shape of the eigenfunctions of the X and z modes about such a static-breather profile in order to calculate its discrete small-oscillation frequency spectrum and such a procedure corresponds to an exact *numerical* dressing of the bare theory. The third regime corresponds to the case where the interaction energy at maximum subkink separation is comparable to the Peierls energy and this is the most difficult case to describe theoretically. Our bare results are not sufficient in this case to account for breather stability with respect to the X motion. One agains needs to incorporate the dressing, but since the breather oscillation is nonlinear, we have no corresponding eigenfunctions for this case. We briefly describe a method to include the dressing to lowest order for such a case.

We order q_l which appears in Eq. (3.3) as follows:

$$q_l \rightarrow q(x,t)=\epsilon^2 q^{(0)}(x,t)+\epsilon^4 q^{(1)}(x,t)+\cdots \tag{5.1}$$

and assume that each space and each time derivative of f and q augment the power of ϵ by one. Substituting Eqs. (3.3) and (5.1) into Eq. (3.2) and expanding the second difference in a Taylor series, we obtain an equation containing powers of ϵ, each coefficient of which must be zero. To lowest order in ϵ we therefore obtain the differential equation

$$\ddot{q}^{(0)}-q^{(0)}_{xx}+V''_{\rm sub}(f)q^{(0)}=\frac{2}{4!}f_{xxxx}\ , \tag{5.2}$$

where subscripts denote partial derivatives with respect to the continuum variable x and the primes on the potential denote derivatives with respect to the argument f. Equation (5.2) for $q^{(0)}$ and the resulting next order differential equation for $q^{(1)}$ have both been solved for the single kink case.[37] For the breather case we must substitute the continuum breather solution ϕ_b for f and then solve Eq. (5.2). When $q^{(0)}$ is found, we construct the new ansatz $Q_l=\bar{f}_l+\bar{q}_l$, where

$$\bar{f}_l=\phi_b(l,t)+q^{(0)}(l,t)\ ,$$

where x is replaced by l again. The $\bar{q}_l$ are new dressing and radiation variables. A new bare theory in the function $\bar{f}_l$ is then expected to yield better results in all regimes discussed above. Although the solution to Eq. (5.2) for a breather has not yet been derived, all solutions to the corresponding homogeneous equation, i.e., the discrete and continuous spectrum, are known exactly[37] and the solution to Eq. (5.2) may take a relatively simple form. Work along these lines is in progress.

We used molecular-dynamics simulations and Fourier-transform techniques to analyze the frequency spectrum of the discrete-breather system for the choice $\Gamma_0=\sqrt{2}$. We examined the frequency range $0.837\leq\omega_b\leq 1.406$ corresponding to breathers whose third harmonic is above the phonon band. We found that only breathers centered on particles are stable in X except in the frequency subrange $0.993\leq\omega_b\leq 1.040$, where breathers for both $X=\frac{1}{2}$ *and* 0 are unstable to the X motion. We do not know if this is due to a fundamental change in the structure of the potential due to discreteness, or if there was some internal resonance in the system which, due to finite numerical accuracy, pushed the breather's center of mass over the small Peierls barrier.

In general, we found that the band-edge phonons were excited by the initial conditions of the simulation which produce combination modes with the breather and its harmonics throughout the spectrum. Since the band-edge phonons cannot be eliminated, Fig. 7 is in this sense a fundamental frequency diagram for the states that exist in the discrete-breather system. We found no evidence of breather subharmonics for the discrete SG case, see Fig. 7.

Molecular-dynamics simulations show that $3\omega_b$ plays a crucial role in determining the lifetime of the discrete breather. When in the phonon band, the third harmonic acts as a powerful source of radiation leading to a breather lifetime of five or six breather oscillations. When the third harmonic is above the phonon band, the lifetime is about 10^4 to 10^5 breather oscillations. We have shown that the transition from the short to long lifetime is extremely sharp and does not depend on the initial breather frequency. In addition, for an infinite chain where the phonon band is truly a continuum of phonon states, we do not expect to find stable discrete breathers even with high frequency because combination modes in the band will always resonate with a phonon mode and radiate energy.

As a final remark, we note that we did not calculate an expression for the breather frequency in the bare approximation. Although it is conceptually simple, the calcula-

tion is rather involved. For example, let us consider only the continuum case for which all the answers are already known. The exact equation of motion for z given by Eq. (2.19d) may be written explicitly as

$$\ddot{z} = -\frac{\Gamma_0^2}{k_b}\tanh(k_b z)\operatorname{sech}^2(k_b z) , \tag{5.3}$$

the solution of which is given by Eq. (2.13). Although z is very useful as a position parameter for the subkinks, it is not useful for calculating the breather frequency even in a small-amplitude (high-frequency) limit since the amplitude z_0 is bounded from below according to Eq. (2.21). Even though we should not need to linearize since the exact solution is known, the attempt itself to carry out a linear calculation makes no sense because of Eq. (2.21). In order to calculate frequencies, we clearly need to use a different variable for which even a linearization of the equation of motion makes sense.

Consider the new variable $u = \sinh(k_b z)$. For the smallest oscillations in $z \approx z_0$, we note that $k_b \to 0$. Therefore, the amplitude of u *does* take on arbitrarily small values and u can be used as a small-oscillation variable if so desired. Instead of linearizing though, we merely transform Eq. (5.3) from z to u and obtain

$$\ddot{u} = \frac{u}{1+u^2}(\dot{u}^2 - \Gamma_0^2) . \tag{5.4}$$

Although Eq. (5.4) is nonlinear, it has a harmonic solution given exactly by the right-hand side of Eq. (2.13). Why then is Eq. (5.4) nonlinear? It is because if we assume a solution $u = A\cos(\omega_b t)$, the amplitude A is not an independent parameter and the nonlinearity forces $A = k_b/\omega_b$. Now it is possible to transform the equation of motion for z for the discrete case to the variable u. The continuum limit of the resulting u equation will, of course, be Eq. (5.4) but will otherwise lead to corrections on Eq. (5.4). Corrections on ω_b may be obtained in this manner and the results will be presented in a forthcoming paper.

[1] J. A. Combs and S. Yip, Phys. Rev. B **28**, 6873 (1983); **29**, 438 (1984).

[2] M. B. Fogel, S. E. Trullinger, A. R. Bishop, and J. A. Krumhansl, Phys. Rev. B **15**, 1578 (1977); J. F. Currie, S. E. Trullinger, A. R. Bishop, and J. A. Krumhansl, *ibid.* **15**, 5567 (1977); S. E. Trullinger, *ibid.* **22**, 418 (1980).

[3] J. C. Fernandez, M. J. Goupil, O. Legrand, and G. Reinisch, Phys. Rev. B **34**, 6207 (1986).

[4] M. J. Rice, Phys. Rev. B **28**, 3587 (1983).

[5] M. Peyrard and M. Kruskal, Physica D **14**, 88 (1984).

[6] C. R. Willis, M. El-Batanouny, and P. Stancioff, Phys. Rev. B **33**, 1904 (1986).

[7] P. Stancioff, C. R. Willis, M. El-Batanouny, and S. Burdick, Phys. Rev. B **33**, 1912 (1986).

[8] R. Boesch and C. R. Willis, Phys. Rev. B **42**, 2290 (1990).

[9] R. Boesch and C. R. Willis, Phys. Rev. B **39**, 361 (1989).

[10] R. Boesch, C. R. Willis, and M. El-Batanouny, Phys. Rev. B **38**, 2284 (1989).

[11] D. K. Campbell, M. Peyrard, and P. Sodano, Physica D **19**, 165 (1986).

[12] R. Ravelo, M. El-Batanouny, C. R. Willis, and P. Sodano, Phys. Rev. B **38**, 4817 (1988).

[13] M. Peyrard and D. K. Campbell, Physica D **19**, 33 (1983).

[14] M. Peyrard and M. Remoissenet, Phys. Rev. B **26**, 2886 (1982).

[15] D. K. Campbell, J. F. Schonfeld, and C. A. Wingate, Physica D **9**, 1 (1983).

[16] S. E. Trullinger, J. Math. Phys. **21**, 592 (1980).

[17] P. Tchofo Dinda and E. Coquet, J. Phys.: Condens. Matter **2**, 6953 (1990), and references therein.

[18] M. Peyrard, J. Math. Phys. **22**, 2986 (1981).

[19] E. Stoll, T. Schneider, and A. R. Bishop, Phys. Rev. Lett. **42**, 937 (1979).

[20] A. R. Bishop, J. Phys. A **14**, 1417 (1981).

[21] Y. Kivshar and B. Malomed, Rev. Mod. Phys. **61**, 763 (1989).

[22] A. Mazor (Ben-Mizrachi) and A. R. Bishop, Physica D **27**, 269 (1987).

[23] M. Taki, J. C. Fernandez, and G. Reinisch, Phys. Rev. B **38**, 3086 (1988); M. Taki and K. H. Spatschek, J. Phys. (Paris) Colloq. **50**, C3-77 (1989); M. Taki, K. H. Spatschek, J. C. Fernandez, R. Grauer, and G. Reinisch, Physica D **40**, 65 (1989).

[24] A. M. Kosevich and A. S. Kovalev, Zh. Eksp. Teor. Fiz. **67**, 1793 (1974) [Sov. Phys. JETP **40**, 891 (1975)].

[25] K. Sasaki, Phys. Rev. B **33**, 2214 (1986).

[26] S. E. Trullinger and K. Sasaki, Physica D **28**, 181 (1987).

[27] C. R. Willis and R. Boesch, Phys. Rev. B **41**, 4570 (1990).

[28] M. Peyrard and A. R. Bishop (unpublished).

[29] O. M. Braun and Y. S. Kivshar, Phys. Rev. B (to be published).

[30] Y. Ishimori and T. Munakata, J. Phys. Soc. Jpn. **51**, 3367 (1982).

[31] P. A. M. Dirac, *Lectures on Quantum Mechanics* (Academic, New York, 1964).

[32] E. Tomboulis, Phys. Rev. D **12**, 1178 (1975).

[33] (a) R. Boesch, P. Stancioff, and C. R. Willis, Phys. Rev. B **38**, 6713 (1988); (b) R. Boesch and C. R. Willis, *ibid.* **42**, 6371 (1990).

[34] C. R. Willis, M. El-Batanouny, R. Boesch, and P. Sodano, Phys. Rev. B **40**, 686 (1989).

[35] S. de Lillo and P. Sodano, Lett. Nuovo Cimento **37**, 380 (1983).

[36] D. K. Campbell and M. Peyrard, in *Chaos/XAOC, Soviet-American Perspectives in Nonlinear Science,* edited by D. K. Campbell (American Institute of Physics, New York, 1990).

[37] R. Boesch (unpublished).